Breaking Rossby Waves in a Model Stratosphere Diagnosed by a Vortex-Following Coordinate System and a Technique for Advecting Material Contours

WARWICK A. NORTON

Centre for Atmospheric Science, Department of Applied Mathematics and Theoretical Physics, University of Cambridge, Cambridge, United Kingdom*

(Manuscript received 28 October 1992, in final form 10 May 1993)

ABSTRACT

This paper presents results from a single-layer, shallow-water, 100-day model integration that reproduces many features of the wintertime stratosphere, particularly in the tropics, more realistically than earlier single-layer integrations. The advective transport of passive tracers by breaking Rossby waves is examined using a new polar-vortex-following coordinate system and a technique for advecting material contours, in which they are followed very accurately using the contour-dynamics algorithm of Dritschel. Unlike any Eulerian tracer advection scheme, the technique for advecting material contours has no numerical diffusion and can handle the ultrafinescale, exponentially shrinking tracer features characteristic of chaotic advective transport or "stirring," which is conspicuous here in the stratospheric "surf zone." The technique may become important as a benchmark for quantitative comparison with Eulerian tracer advection schemes, such as those used in general circulation models.

Averages with respect to the vortex-following coordinate system give a clearer picture of the gross features of the tracer transport than conventional Eulerian zonal averages, because the reversible displacements associated with undulating Rossby waves are largely eliminated. Results indicate that the edge of the polar vortex acts as a flexible, "Rossby elastic" barrier to eddy transport of air from the surf zone into the vortex, with air well inside the vortex completely isolated for the entire 100 days. This last point is precisely demonstrated by results from the technique for advecting material contours. Erosion of material from the vortex during days 30 to 100 of the model integration was not more than about 16% of the area of the model's surf zone, counted as the area between 30°N and 60°N. The model integration also shows, more realistically than earlier single-layer integrations, a partial barrier to exchange of air between the tropics and middle latitudes.

Results using the technique for advecting material contours also show that material contours in the surf zone lengthen exponentially rapidly with an *e*-folding time of about 4 days during the first 30 days. Material contours in the tropics lengthen only slowly, the contour farthest within the tropics lengthening by a factor of only 2 during the first 30 days. Material contours embedded in the vortex edge behave in an almost purely undular manner and hardly lengthen at all, except near the end of 100 days of integration when the vortex is violently disturbed and relatively strongly eroded albeit still showing a perfectly isolated core. The minimum distance between contours is also examined and shows exponentially shrinking behavior in the surf zone with a fastest *e*-folding time of about 1 day, dominated by what happens in the regions of strongest stirring. The relevance to real stratospheric ozone depletion and the "flowing processor hypothesis" is discussed.

1. Introduction

The dynamics of the extratropical winter stratosphere is dominated by the polar vortex. Studies from satellite data (e.g., McIntyre and Palmer 1983, 1984; Al-Ajmi et al. 1985; Clough et al. 1985; Leovy et al. 1985) have shown that the vortex can be highly disturbed by Rossby wave breaking events. These events erode the vortex, transporting vortical air into middle latitudes and steepening the isentropic gradients of potential vorticity (PV) that mark the edge of the vortex. These events also strongly stir, or chaotically advect, the air in middle latitudes, irreversibly deforming PV contours and material contours and creating a midlatitude "surf zone" (McIntyre and Palmer 1983, 1984).

In the cold air within the vortex, heterogeneous reactions on polar stratospheric clouds can produce chemically perturbed conditions with high concentrations of reactive inorganic chlorine, which in the presence of sunlight destroys ozone (e.g., Solomon 1990). It has been hypothesized (e.g., Tuck et al. 1992) that the transport of this chemically perturbed, or chlorine-activated, air out of the vortex is an important factor in the recently observed midlatitude ozone decline (Stolarski et al. 1991, 1992 and references therein). The

* The Cambridge Centre for Atmospheric Science is a joint initiative of the Department of Chemistry and the Department of Applied Mathematics and Theoretical Physics.

Corresponding author address: Dr. W. A. Norton, Atmospheric, Oceanic and Planetary Physics, Department of Physics, Clarendon Laboratory, Parks Road, Oxford, UK, OX1 3PU.

vortex is hypothesized to be a "flowing processor," feeding large amounts of activated air to middle latitudes in the lower stratosphere; see also Tuck (1989), Proffitt et al. (1990), and, for instance, the recent discussion by Randel (1993). Therefore, it is important to understand the processes that might transport air out of the vortex, and to understand the isentropic stirring that reduces the scale of this vortical air so that it can mix with ambient midlatitude air. The whole "mix-down" process seems likely to occur on time scales of the order of a week or two (McIntyre 1990), comparable to some of the relevant chemical time scales and possibly leading to accelerated chlorine deactivation.

There have been a number of studies examining stratospheric polar vortex dynamics in various single-layer models, for example, Juckes and McIntyre (1987, hereafter referred to as JM87), Juckes (1989, hereafter referred to as J89), Salby et al. (1990), and Polvani and Plumb (1991). They have provided high-resolution views of what the transport and isentropic stirring might look like in the real stratosphere. In particular, they have shown how Rossby wave breaking events can produce many small-scale filaments near the edge of the polar vortex. Chemical data from the airborne ozone expeditions (e.g., Tuck et al. 1992 and references therein) have confirmed the existence of small-scale features near the edge of the real stratospheric vortex, having the chemical signature of vortex air and plausibly corresponding to the model filaments. An important suggestion from the study of JM87 was that, because of the "Rossby elasticity" associated with the PV gradients at the vortex edge and because of the strong shear just outside it, the polar vortex might act approximately as an isolated air mass, resisting zonally asymmetric incursions of air from its surroundings. This might be a significant factor in creating the conditions that allow ozone destruction to take place, especially the massive destruction observed within the Antarctic vortex. There was also a suggestion that the outward transport of vortical air by erosion into the surf zone might be small.

The aim of this paper is to analyze these and other aspects of the transport and stirring in a more realistic model stratosphere, using a new quasi-Lagrangian, vortex-following coordinate system, and a technique for advecting material contours that allows some fundamental properties of the stirring to be studied for the first time and erosion rates to be credibly estimated. The model integration used here, a 100-day shallow-water integration, has a more realistic surf zone and tropics than in earlier model integrations, in which the surf zone extended unrealistically far into the tropics.

The technique for advecting material contours by the model's velocity field uses a highly sophisticated particle redistribution algorithm, adopted from the contour dynamics algorithm of Dritschel (1989). This technique permits the advection of material contours, hence passive-tracer isopleths, to be followed with almost perfect accuracy. It vividly reveals the characteristic fine detail produced in tracer fields by the stirring associated with breaking Rossby waves. Such detail (Figs. 14 and 15) is practically impossible to resolve with any conventional Eulerian tracer-advection scheme. Waugh and Plumb (1994) have independently introduced the same technique and applied it to GCM and meteorological wind data. For the remainder of this paper I shall follow their terminology and refer to the technique as "contour advection."

The improved realism of the present model integration appears to have resulted from a combination of three factors not simultaneously present in earlier integrations. The first is a smaller Rossby deformation radius. In JM87, for instance, the deformation radius was infinite, producing very long range interactions and hence a more disturbed tropics. Juckes (1989) used a mean layer thickness of 8 km, hence midlatitude deformation radius ~2800 km, while the present integration uses 4 km, hence midlatitude deformation radius ~2000 km. The second factor is the use of a spherical rather than a hemispherical model domain. The presence of an effective solid wall at the equator in a hemispherical model tends to reflect waves and to produce a more disturbed tropics. The third factor is an initial condition leading to a smaller polar vortex, arguably a more typical size for the lower and middle stratosphere.

Section 2 of this paper presents the model equations and shows some PV maps from the integration. Section 3 shows the results of introducing three different passive tracer fields into the integration and following them by means of the model's Eulerian advection scheme. Section 4 describes the new vortex-following coordinate system, shows some averaged diagnostics using it, and compares them with alternative diagnostics including conventional Eulerian averages. Section 5 introduces the contour advection technique, illustrating its far more accurate handling of a passive tracer field including the generation of ultrafinescales (again, see Figs. 14 and 15). Section 6 presents quantitative information about the exponentially fast rates at which tracer scales shrink in the surf zone, and material contours lengthen. These rates are fundamental properties of turbulence and chaotic advection. The contour-advection results are also used in section 6 to address the issue of polar vortex isolation. Section 7 discusses the relevance to real stratospheric ozone depletion and the "flowing processor hypothesis."

2. Model description

The model code is the same as used by J89, that is, the Reading pseudospectral code solving the shallow-water equations on the sphere. The shallow-water vorticity, divergence, and mass continuity equations are

$$\frac{\partial \zeta}{\partial t} = -\nabla\cdot(\mathbf{v}\zeta_a) + \kappa\nabla^6\zeta, \qquad (1a)$$

$$\frac{\partial \delta}{\partial t} = \mathbf{k}\cdot\nabla \times (\mathbf{v}\zeta_a) - \nabla^2\left(\frac{u^2 + v^2}{2}\right) - g\nabla^2(\sigma + H) + \kappa\nabla^6\delta, \quad (1b)$$

$$\frac{\partial \sigma}{\partial t} = -\nabla\cdot(\mathbf{v}\sigma) + \frac{1}{\tau}(\sigma_0 - \sigma) + \kappa\nabla^6\sigma, \quad (1c)$$

where ζ is the vorticity, $\zeta_a = f + \zeta$ the absolute vorticity, δ the divergence, σ the layer thickness, and $\mathbf{v} = (u, v)$ the velocity field. The numerical hyperdiffusion coefficient κ is set to 2.6×10^{24} m^6 s^{-1}; H is the height a specified bottom topography, which forces the flow. Here it is given the spatial and temporal variation

$$H = H_0 A(t) B(\phi) C(\lambda), \quad (2a)$$

where t is time, ϕ latitude, and λ longitude. Also, for $t \leq 20$ with t in days,

$$A(t) = \begin{cases} \frac{1}{2}\left(1 - \cos\frac{\pi t}{4}\right), & t < 4 \\ 1, & 4 \leq t < 16 \\ \frac{1}{2}\left(1 + \cos\frac{\pi(t-16)}{4}\right), & 16 \leq t < 20, \end{cases} \quad (2b)$$

$$B(\phi) = \begin{cases} \frac{\cot^2\phi}{\cot^2\phi_0}\exp\left(1 - \frac{\cot^2\phi}{\cot^2\phi_0}\right), & \phi \geq 0 \\ 0, & \phi < 0, \end{cases} \quad (2c)$$

$$C(\lambda) = -\sin\lambda + 0.2\sin 2\lambda, \quad (2d)$$

where $H_0 = 0.72$ km and $\phi_0 = 45°$; $B(\phi_0)$ has a value of unity. For $20 < t \leq 40$, (2b) is used with $(t - 20)$ in place of t, and so on, repeating the cycle periodically. This form of forcing with wave 1 and some wave 2 has been chosen to mimic the upward-propagating, planetary-scale Rossby waves that, in accordance with the Charney–Drazin hypothesis, are typical of conditions found in the middle stratosphere.

The diabatic relaxation term in the mass continuity equation (1c) is included to represent crudely the "radiative spring" (Fels 1985) of the real atmosphere. The relaxation time scale τ is 20 days. The "radiative equilibrium" distribution σ_0 is taken as the initial, axisymmetric mass distribution implied by gradient-wind balance and the PV field at day 0 shown in Fig. 1. Potential vorticity in this model is defined as

$$Q = \frac{\zeta_a}{\sigma} \quad (3)$$

and is materially conserved except for the effects of the diabatic relaxation term in (1c) and numerical hyperdiffusion. The initial, axisymmetric PV distribution corresponds to a wind distribution that had a westerly jet of 50 m s^{-1} centered at 60°N and weak easterlies in the Southern Hemisphere. The initial mass distribution has global-mean layer thickness of 4 km. A pseudospectral method with centered time differencing is used to integrate Eq. (1).

The model is integrated for 100 days at spectral truncation T127. Figure 1 shows contour plots of the first 30 days' evolution of the PV field. At day 10, the topographic forcing is at its maximum amplitude, and we see the classic wave-1 Rossby wave-breaking signature. The vortex is displaced off the pole and there is a tongue of high PV air being drawn out from the vortex with sideways overturning, or folding, of PV contours in the surf zone. At day 20 the forcing has decreased to zero, and the vortex has returned to a position approximately over the pole. However, there is a large undular disturbance on the edge of the vortex, in which wave 3 is conspicuous, and there has clearly been irreversible deformation of PV contours in the surf zone. At day 30 the forcing is again at its maximum amplitude, and the surviving part of the vortex has again moved off the pole. It has been visibly eroded by this stage, as can be seen from the sharp PV gradient that now marks part of the outer edge of the vortex.

Figure 2 shows the evolution of the PV field between days 40 and 100. At all times there are sharp PV gradients at the outer edge of the vortex. However, at no stage do the sharp gradients extend all the way around the vortex; this contrasts with some of the earlier model results. Note, for instance, the contour shapes at 45°N, 30°W on day 60 (counting 0° as the line from the center to bottom of the figures), marking an erosion event. Such events typically take material from the vortex periphery only, as has also been seen in countless idealized vortex-dynamics studies (e.g., Legras and Dritschel 1993).

There are also some transitory regions of sharp gradients in the surf zone. Note regions of somewhat steeper gradients in the subtropics, for example, day 80, 90°E to 180°. The vortex at day 100 is very distorted and completely off the pole. There is a small anticyclonic vortex near 70°N, 45°E, which appears to be pulling a small tongue of air out from the polar vortex. Further inspection of times near day 100 shows that this anticyclonic vortex developed from low PV air that had been advected round the polar vortex from the tropics, in the manner first described by Leovy et al. (1985); we return to this point in the Discussion.

3. Eulerian tracer experiments

A qualitative overview of the transport and stirring in the model, highlighting different regions, was obtained by including three passive chemical tracer fields in the model integration. The tracers were initialized as small Gaussian-shaped blobs with the first, tracer A, centered on the pole and well inside the vortex; the

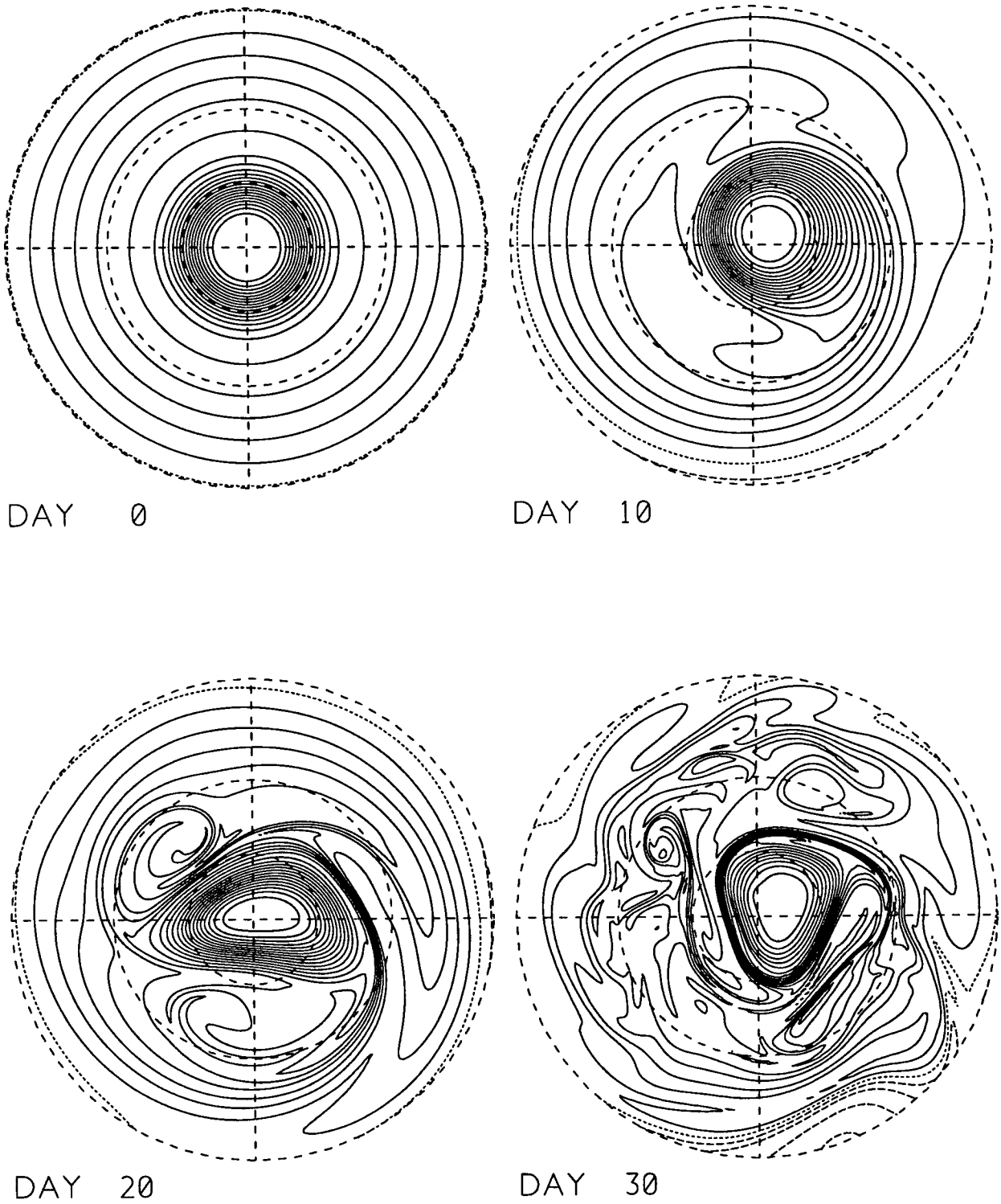

FIG. 1. Potential vorticity for days 0 to 30 from integration of shallow-water equation model. Contour interval is 4×10^{-9} m^{-1} s^{-1}. Positive PV values, solid contours; zero PV value, dotted contour; negative PV values, dashed contours. Polar stereographic projection and dashed circles are at 0°N, 30°N, and 60°N. The zero of longitude, for descriptive purposes in the text, is the line from the center to bottom of the figures.

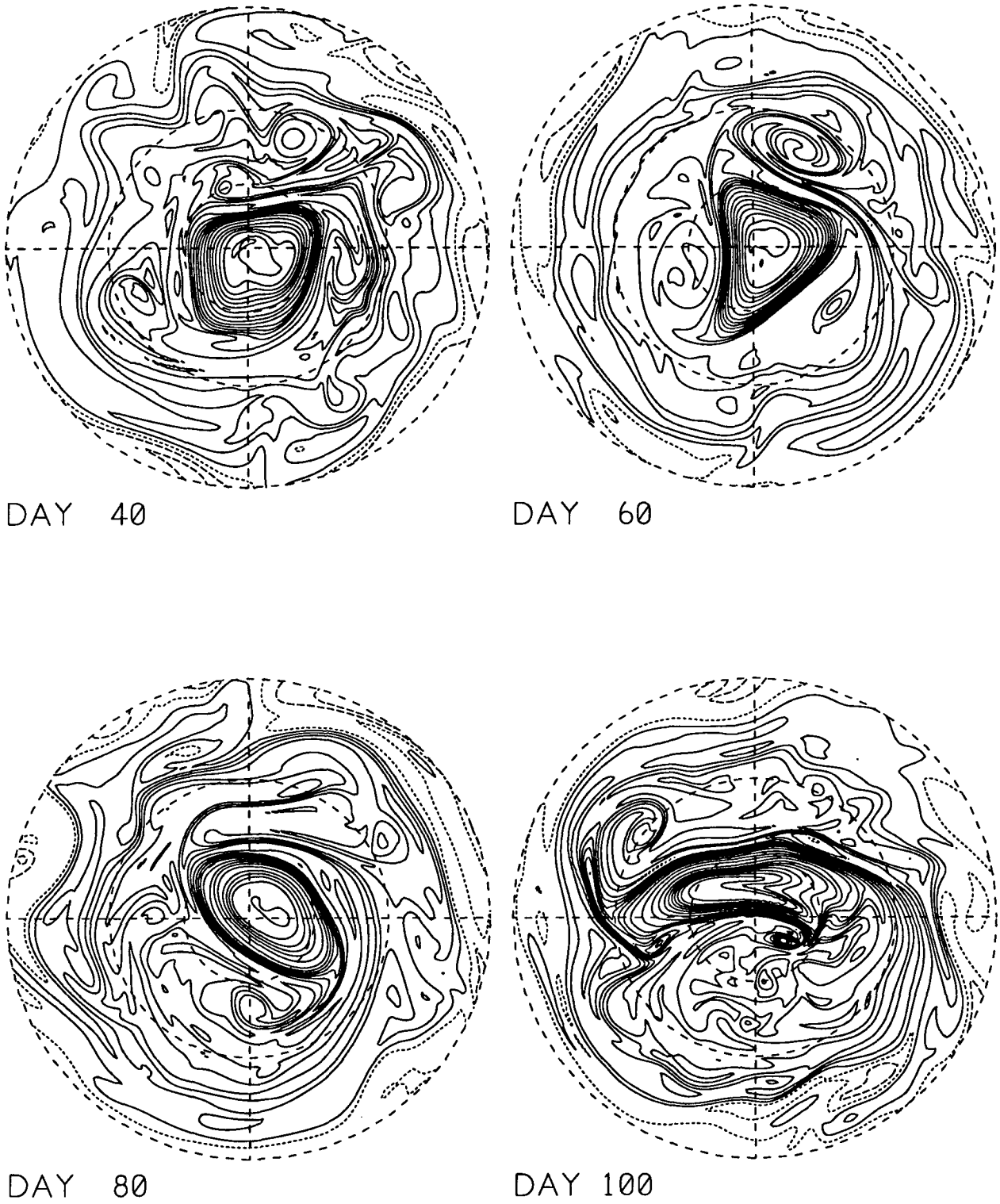

FIG. 2. Same as Fig. 1 but for days 40 to 100.

second, tracer B, centered at 45°N in what will become the surf zone; and the third, tracer C, centered on the equator. The same pseudospectral scheme as used by the dynamics was used for advecting the tracers; cf. the far more accurate contour advection results of section 5.

Figure 3 shows the initial conditions and evolution of tracer A, in grayscale form. This tracer remains mostly as one blob. Comparing Fig. 3 with the PV in Figs. 1 and 2 suggests that it remains almost totally inside the polar vortex. This is particularly striking on day 100, when the vortex is very disturbed. The small amount eroded from the vortex, just visible in Fig. 3, day 100, is mainly a numerical artifact associated with "Gibbs fringes" produced by the hyperdiffusion and the spectral representation.

Figure 4 shows the initial conditions and evolution of tracer B. This tracer has an evolution very different from that of tracer A. Since the initial isopleths of this tracer are not aligned along streamlines, there is initially strong dispersion of the tracer as it gets sheared out and wound round the vortex. At day 20, spiral struc-

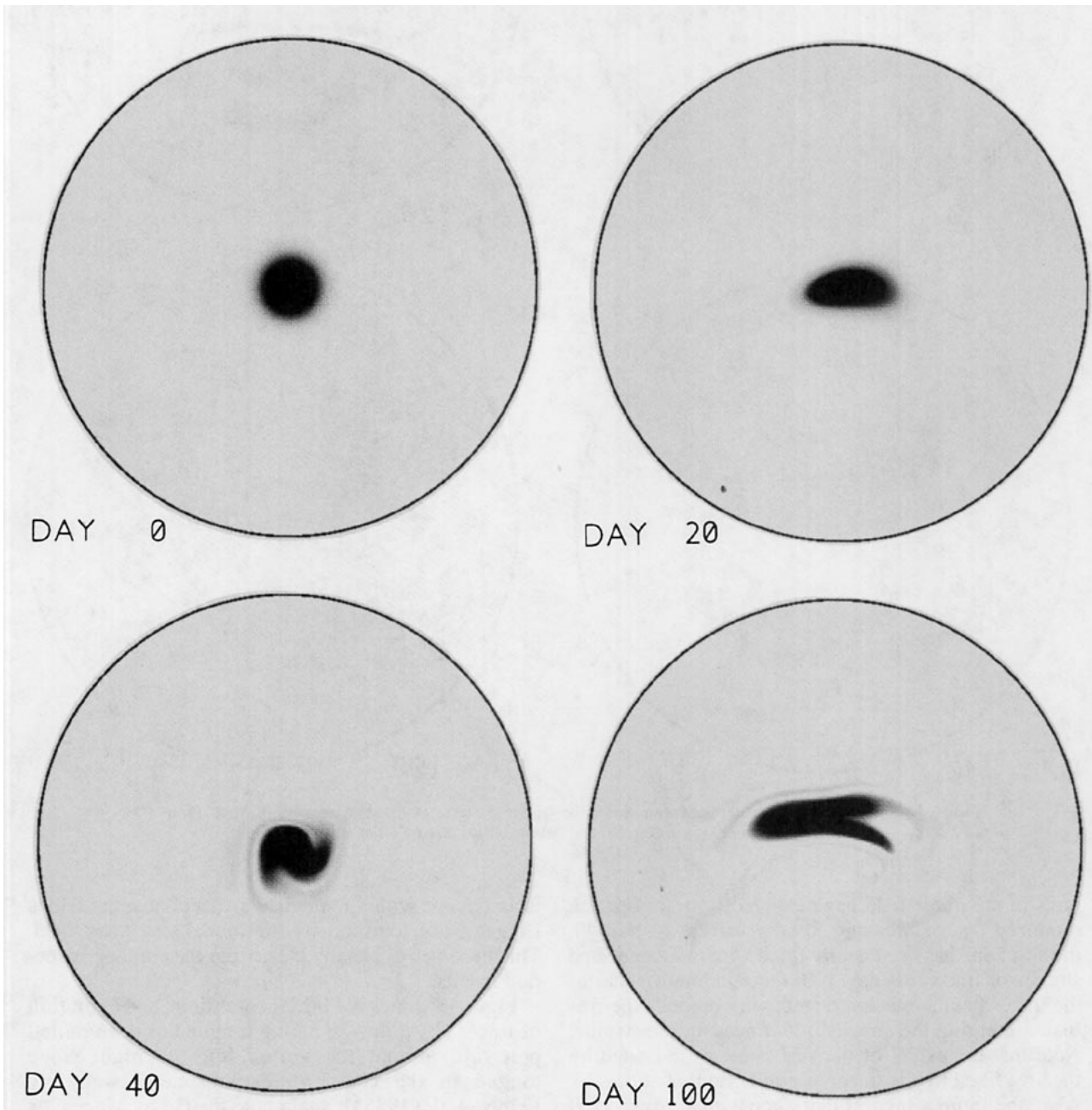

FIG. 3. Evolution of passive tracer field with initial distribution centered on the north pole showing days 0, 20, 40, and 100. White represents mixing ratios of 0 and below; black, mixing ratios 0.1 and above.

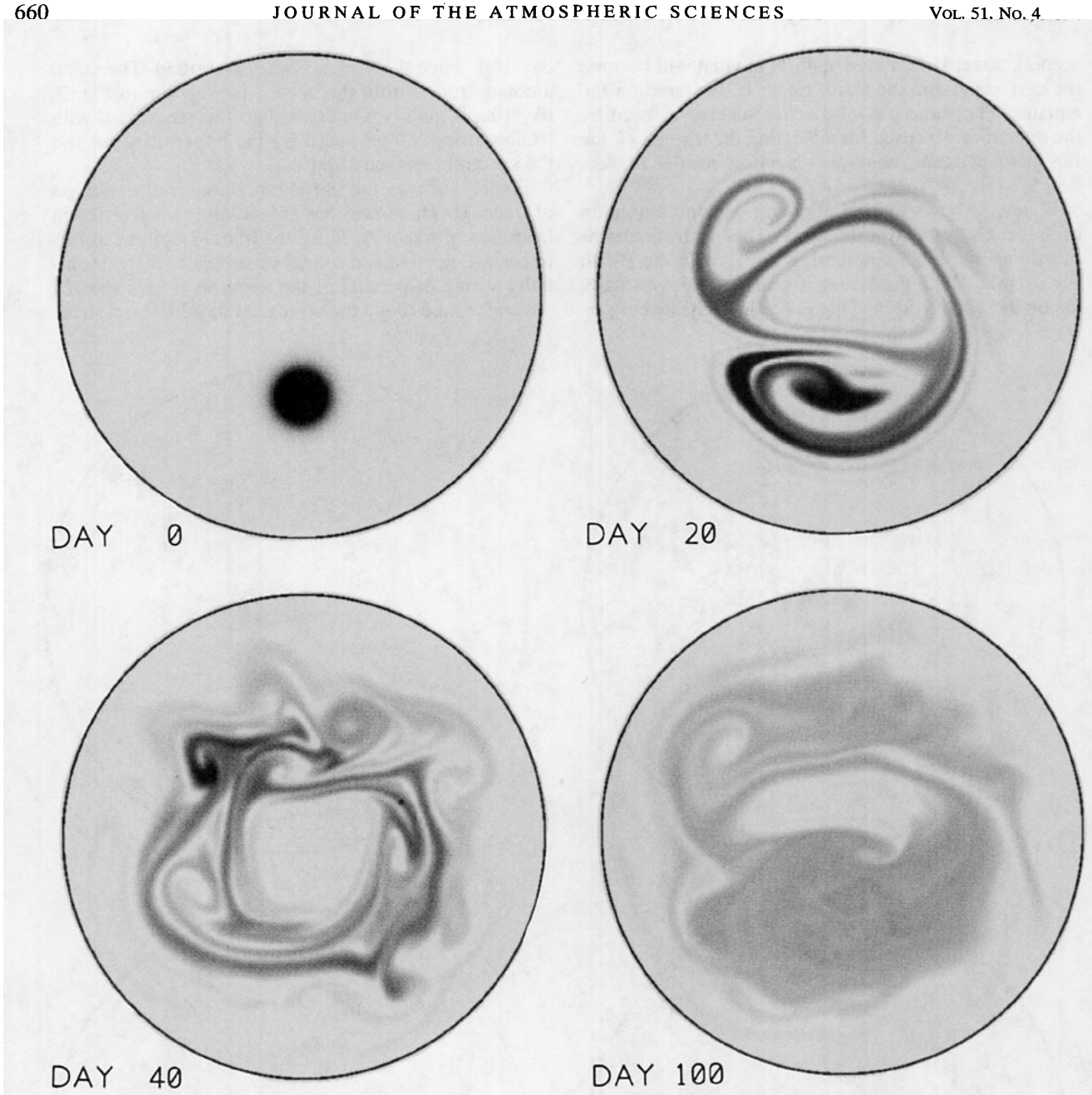

FIG. 4. Evolution of passive tracer field with initial distribution centered at 45° showing days 0, 20, 40, and 100. White represents mixing ratios of 0 and below; black, mixing ratios 0.1 and above.

tures in the tracer field have evolved from the stirring produced by the breaking Rossby waves. At day 40, the surf zone has been nearly filled with interconnected streaks of tracer. At day 100, the maximum value of the tracer field is much reduced, with model hyperdiffusion merging the streaks into a near uniform value. Note that the extent of the surf zone, as indicated by the area filled by the tracer, is similar to that at day 40. Also, the figures suggest that almost none of tracer B gets into the polar vortex; we return to this point in section 6. It turns out that what does appear to get in is associated with a numerical artifact (note the Gibbs fringes), not transport by the model's velocity field. This becomes especially clear from the contour advection results.

Figure 5 shows the initial conditions and evolution of tracer C. At day 20 a long tongue has been pulled poleward around the vortex [cf. the high ozone tongue in the classic midstratospheric study by Leovy et al. (1985)]; again note the Gibbs fringes. At day 40 there are three small patches of high concentration in the Northern Hemisphere, and there is more

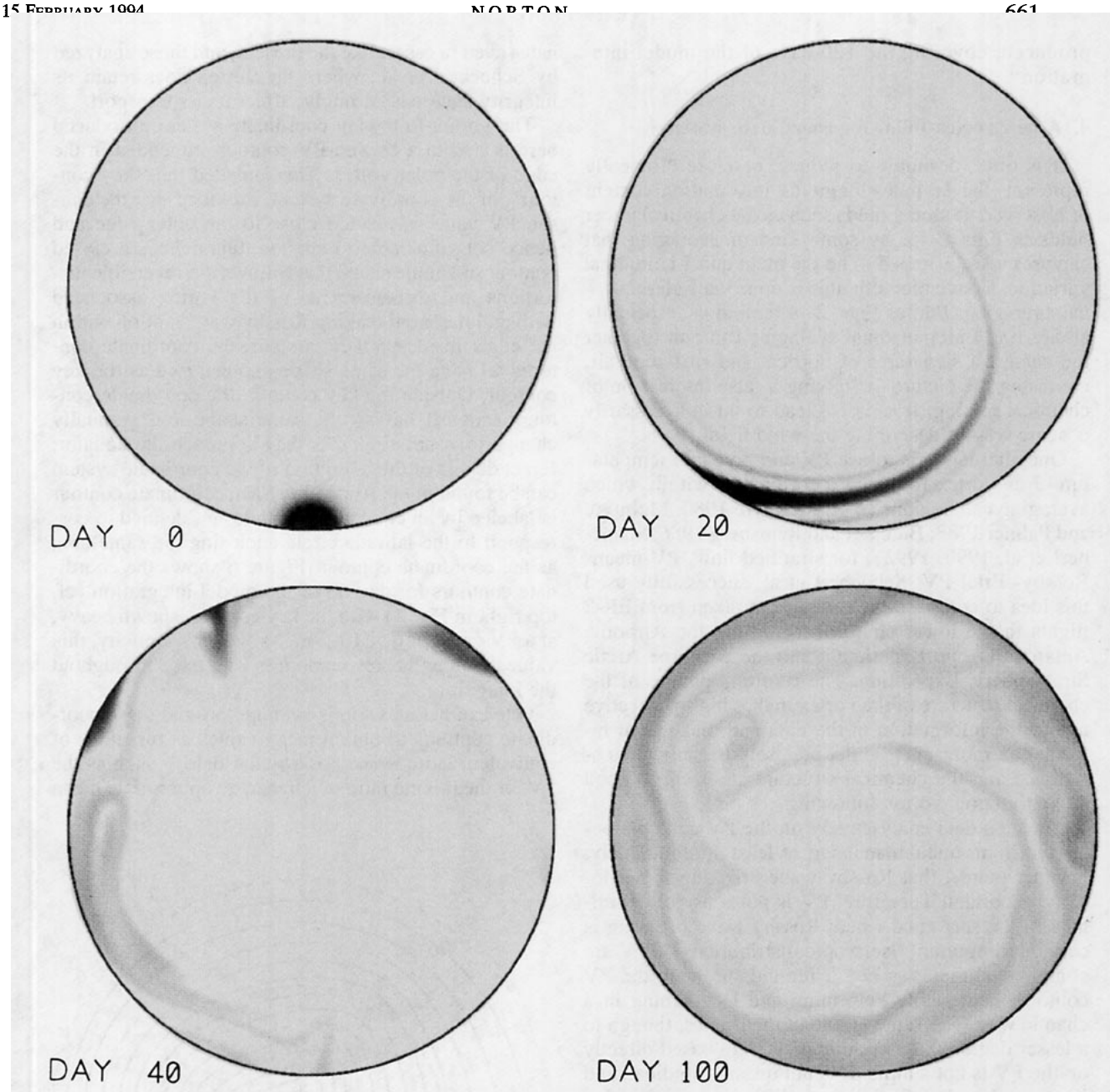

FIG. 5. Evolution of passive tracer field with initial distribution centered on the equator showing days 0, 20, 40, and 100. White represents mixing ratios of 0 and below; black, mixing ratios 0.1 and above.

tracer in the tropical Southern Hemisphere (not shown). Thus, this tracer disperses only slowly through and from the tropics, indicating that the stirring is much weaker in this region than in the surf zone. At day 100 the tracer has mostly filled a band in the tropics, reminiscent of many observational studies of stratospheric sulfuric acid aerosol from tropical volcanic eruptions (e.g., McCormick and Veiga 1992; Stowe et al. 1992). There is a weak and intermittent transport from the tropics into the surf zone, by what might be called subtropical erosion. An example is given by the thin band extending from approximately 135°E to 135°W on day 100, showing up light and dark, respectively, in Figs. 4 and 5. This phenomenon is associated with displacements of the polar vortex and is discussed further in section 7.

The character of the midlatitude surf zone as the zone of strongest stirring becomes especially conspicuous in an animated display. A color video showing animated versions of Figs. 1–5 has been

produced, covering the 100 days of the model integration.[1]

4. A new vortex-following coordinate system

It is often desirable to reduce, or more efficiently represent, the latitude–longitude information content of observed or model fields such as the chemical tracer fields in Figs. 3–5, by some kind of averaging that captures what is hoped to be the main quasi-latitudinal variation. Conventionally, this is done via Eulerian zonal averaging. But, as Figs. 2–4 remind us, especially at day 100, Eulerian zonal averaging can blur together the chemical signatures of vortical and surf-zone air, confusing the picture and giving a false impression of chemical mixing. It can also lead to an unnecessarily obscure way of describing the wind field.

One alternative is to use PV and potential temperature θ as vortex-following coordinates, within which averaging can be done (e.g., McIntyre 1980; McIntyre and Palmer 1983; Butchart and Remsberg 1986; Schoeberl et al. 1990, 1992); for stratified flow, PV means Rossby–Ertel PV. Schoeberl et al. successfully used this idea to composite chemical data taken from ER-2 flights in the lower stratosphere during the Airborne Antarctic Ozone Experiment and the Airborne Arctic Stratospheric Expedition. The resulting picture of the chemical structure of the vortex makes highly effective use of the information in the data and makes that information more intelligible, precisely because the coordinate and the chemical structure are both, to good approximation, vortex following.

But such data analyses rely on the PV contours behaving in an undular manner, at least approximately; in other words, that Rossby wave breaking is not locally important. Therefore, PV is not a useful coordinate in the surf zone where Rossby wave breaking is certainly important. Isentropic distributions of PV are complicated there, as Fig. 2 reminds us, with the PV contours continually deforming and lengthening in a chaotic way. The same is true in the tropics, though to a lesser degree. So a coordinate system based directly on the PV is not simple. It is not quasi-latitudinal, and it cannot describe, for instance, distance from the edge of the vortex.

A new coordinate system is therefore introduced, which retains the vortex-following features of a PV coordinate but achieves a simple shape in the surf zone, by reverting smoothly to a monotonic, quasi-latitudinal coordinate not tied to the chaotic PV field there. Inevitably, any such coordinate system has an ad hoc character, and it still has to rely on the edge of the vortex being approximately undular. But the only alternative is to accept the limitations of Eulerian or PV coordinates even in cases, like the present, and those analyzed by Schoeberl et al., where the vortex does retain its integrity and does, strongly, affect tracer transport.

The vortex-following coordinate system introduced here is tied to a chosen PV contour embedded in the edge of the polar vortex. This is called the "key contour" of the coordinate system. Provided that the chosen PV value is not too close to the outer edge and hence not vulnerable to erosion, this defines a closed contour of simple shape that follows the reversible distortions and displacements of the vortex associated with undular, nonbreaking Rossby wave motion within the edge. Inside the key contour, the coordinate contours all have the same shape and centroid as the key contour. Outside the key contour, the coordinate contours start off having the same shape, but gradually change to zonal circles as they approach the equator. Exact details of the definition of the coordinate system can be found in the Appendix. Each coordinate contour is labeled by an equivalent latitude, ϕ_e, defined to correspond to the latitude circle enclosing the same area as the coordinate contour. Figure 6 shows the coordinate contours for day 60 of the model integration (cf. top right in Fig. 2) with the key contour, shown heavy, at a PV value of 6×10^{-8} m^{-1} s^{-1}. For simplicity, this value defining the key contour is kept fixed throughout the integration.

One can define various averages around these coordinate contours to obtain mean values as functions of equivalent latitude ϕ_e. For a scalar field χ such as the PV, or the mixing ratio of a tracer, an appropriate mean

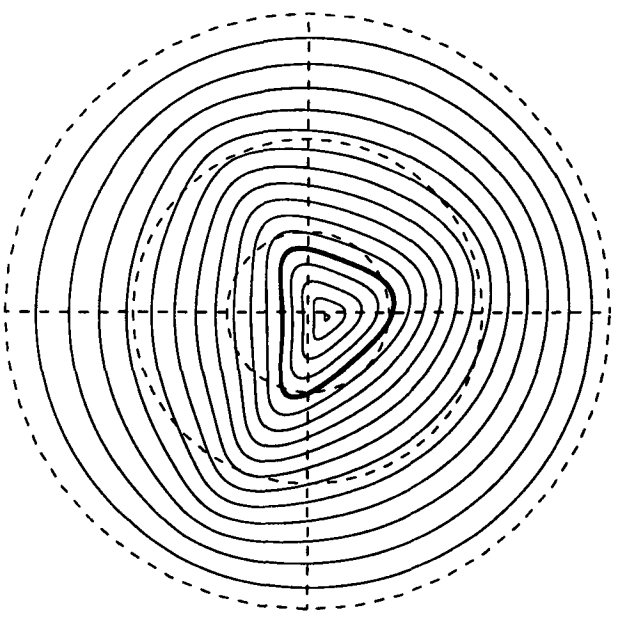

FIG. 6. Vortex-following coordinate system at day 60, showing contours of equally spaced pseudolatitude; see section 4 and Appendix. The heavy contour is the key contour.

[1] VHS cassettes (PAL or NTSC) are available from the author for a nominal fee to cover production costs.

value $\tilde{\chi}$ that respects the additivity of the tracer substance can be defined as the mass-weighted mean

$$\tilde{\chi}(\phi_e) = \frac{\oint \chi(l, \phi_e) w(\phi_e) \sigma dl}{\oint w(\phi_e) \sigma dl}, \qquad (4)$$

where l is distance along a contour, and $w(\phi_e)$ is the distance between contours so that wdl is the area element and $w\sigma dl$ is the mass element. Figure 7 shows the mean PV in this sense, $\bar{Q}$, as a function of equivalent latitude ϕ_e and time t for the model integration. The heavy line indicates the equivalent latitude of the key contour. The steep gradient around 60°N corresponds the edge of the vortex. Note for instance how the area of vortex decreases with time; this is due to the erosion of material from the vortex periphery noted earlier. The area of the surf zone increases both from vortex erosion and from subtropical erosion, especially during the first 30 days when the surf zone expands (cf. Leovy et al. 1985).

One can also define a mean alongcontour wind, $\breve{u}$, as the relative circulation around a contour divided by the length of the contour,

$$\breve{u}(\phi_e) = \frac{\oint \mathbf{v}(l, \phi_e) \cdot d\mathbf{l}}{\oint dl}, \qquad (5)$$

where $d\mathbf{l}$ is tangent to the contour. Figure 8a shows $\breve{u}$ as a function of equivalent latitude and time. In this coordinate system the mean westerly jet shows no large changes over the 100 days of the integration. This is strikingly different from the behavior of the Eulerian zonal-mean zonal wind $\bar{u}$. The latter (Fig. 8b) does show large changes near the pole, even easterlies at day 100, in the manner familiar from the literature on stratospheric warmings.

Both the $\breve{u}$ and the $\bar{u}$ behavior are in accordance with the predictions of wave–mean flow interaction theory. The Eulerian mean, $\bar{u}$, includes the reversible, transient changes associated with undular PV contour behavior,

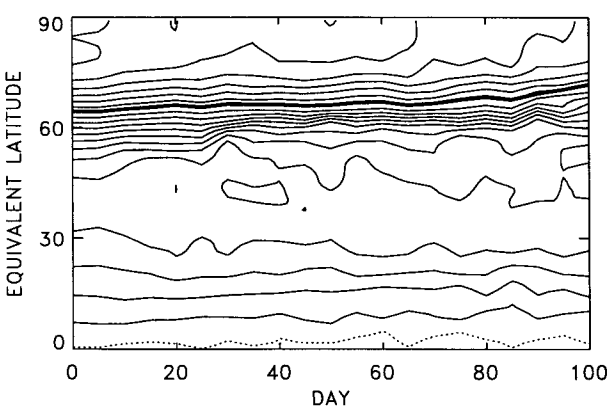

FIG. 7. Mean potential vorticity in vortex-following coordinate system as function of equivalent latitude and time. Contour interval is 4.6×10^{-9} m^{-1} s^{-1}. The heavy line is the position of the key contour. Dotted contour is zero PV value.

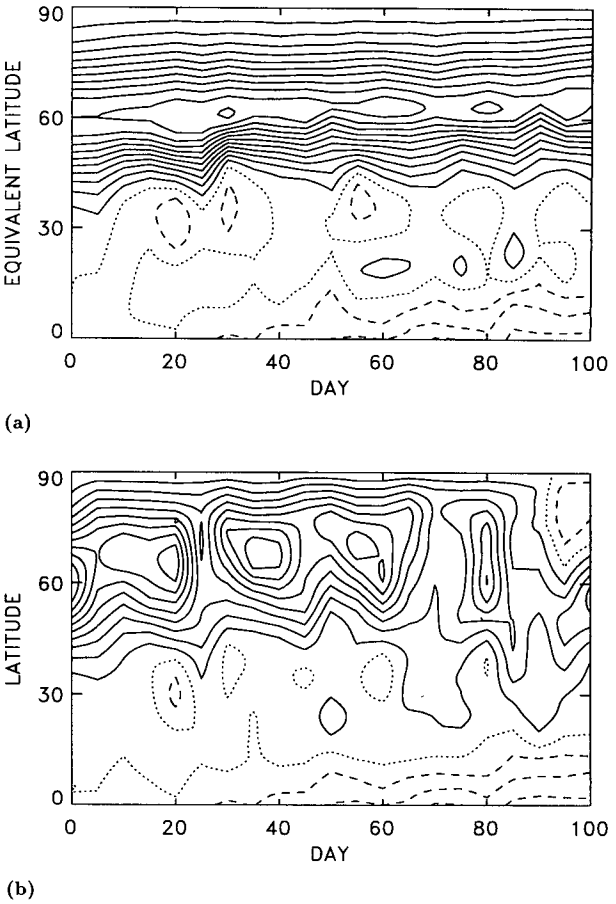

FIG. 8. (a) Mean alongcontour wind in vortex-following coordinate system, defined by Eq. (5), as function of equivalent latitude and time. (b) Eulerian zonal-mean zonal wind as a function of latitude and time. Contour interval is 5 m s^{-1}. Westerlies, solid contours; zero wind line, dotted contour; easterlies, dashed contours.

including wave-1 disturbances displacing the entire vortex off the pole (e.g., McIntyre 1982; Palmer and Hsu 1983). The quantity $\breve{u}$, by contrast, more cleanly isolates the irreversible, quasi-permanent mean flow changes, dominated here by Rossby wave breaking and the irreversible rearrangement of PV, that take place mainly outside the vortex. Such changes are conspicuous (in both $\breve{u}$ and $\bar{u}$) between 30°N and 45°N during the first 30 days, when the surf zone first expands, and in the deep tropics during days 20–100, where Rossby wave breaking is much slower and weaker and rearranges PV more gradually. The correctness of this picture and its relation to wave–mean flow theory has been checked by additional calculations, including calculations of absolute circulation on material contours not presented here.

Another interesting dynamical field to examine is the mean diabatic relaxation term or mean mass source or sink, that is, the vortex-following mean of the second term on the right-hand-side of Eq. (1c). Since that

equation is in flux form, an area mean is used, that is, the mean is taken as in Eq. (4) except that the factors σ are omitted from numerator and denominator. Figure 9 shows the result. There is a mean mass source in the tropics (solid contours), and a mean mass sink reaching a maximum near the edge of the vortex (dashed contours). Therefore, there is a mean mass flux in the layer from the tropics to high latitudes. These features are the model's counterpart to the real atmosphere's diabatic circulation with, presumably, the extratropical mass outflow going mainly downward (Haynes et al. 1991), and the tropical inflow coming mainly upward, contributing to global stratosphere–troposphere exchange.

The mass source region at the highest latitudes is strongest during topographic forcing periods, after days 0, 20, 40, etc. The vortex is then displaced off the pole, and consequently the diabatic relaxation is trying to fill in the small layer thickness associated with the vortex. It is not clear to what extent this aspect of the model resembles the real atmosphere, as opposed to being a consequence of the artificial topographic forcing and artificial diabatic relaxation.

Figure 10 shows the mass-weighted means, $\tilde{\chi}_A$, $\tilde{\chi}_B$, $\tilde{\chi}_C$, of the mixing ratios χ_A, χ_B, χ_C of the tracers A, B, C as a function of equivalent latitude and time. Figure 10a shows how tracer A remains mostly inside the vortex. Figure 10b shows how tracer B rapidly spreads throughout the surf zone but does not extend into the vortex, nor much into the tropics. (The bull's-eyes near day 0 arise because data are plotted only at 5-day intervals.) Figure 10c shows how tracer C remains mostly in the tropics, the first approximation to the observed behavior of tropical volcanic injections.

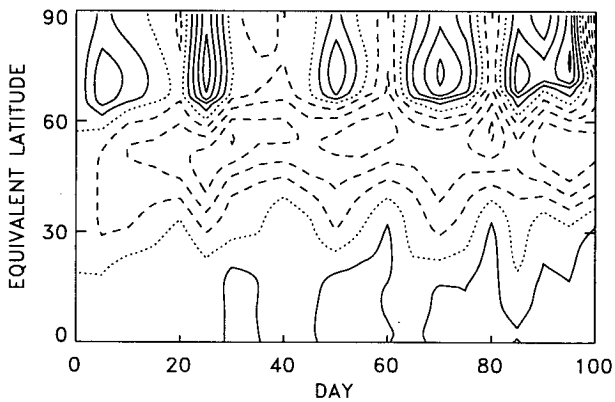

FIG. 9. Mean diabatic mass source or sink in the vortex-following coordinate system, plotted as a function of equivalent latitude and time. The mean of the diabatic relaxation term $\tau^{-1}(\sigma_0 - \sigma)$ is taken as in Eq. (4) except that the factors σ are omitted from numerator and denominator. The contour interval is 5 m day^{-1}, equivalently 0.125% per day of the mean layer depth, 4 km. Positive values (mass source), solid contours; zero value, dotted contour; negative values (mass sink), dashed contours.

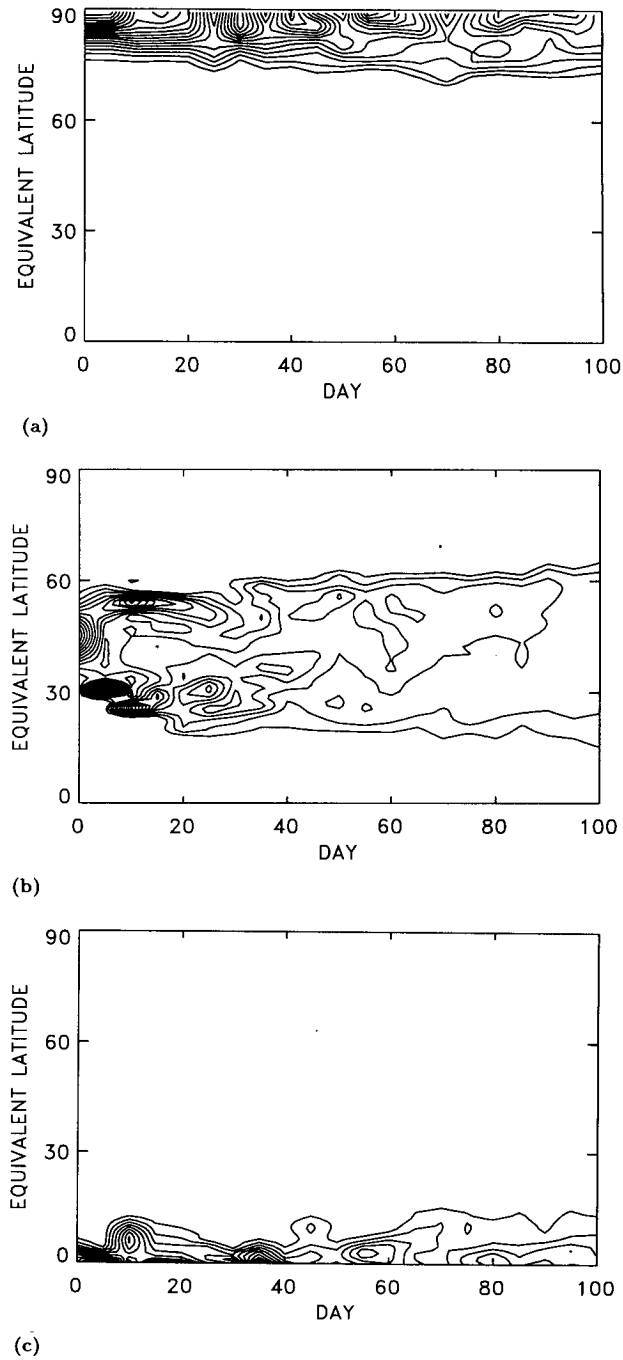

FIG. 10. Mean tracer mixing ratios in vortex-following coordinate system, defined by Eq. (4), as functions of equivalent latitude and time for (a) tracer A: contour interval 0.05, (b) tracer B: contour interval 0.004, and (c) tracer C: contour interval 0.002.

Figure 11 shows the amounts of the tracers [mass-weighted mean of the tracer mixing ratio, Eq. (4), times cosine of equivalent latitude] as functions of equivalent latitude at day 0 (Fig. 11a) and at day 80 (Fig. 11b). Comparison of the midlatitude regions

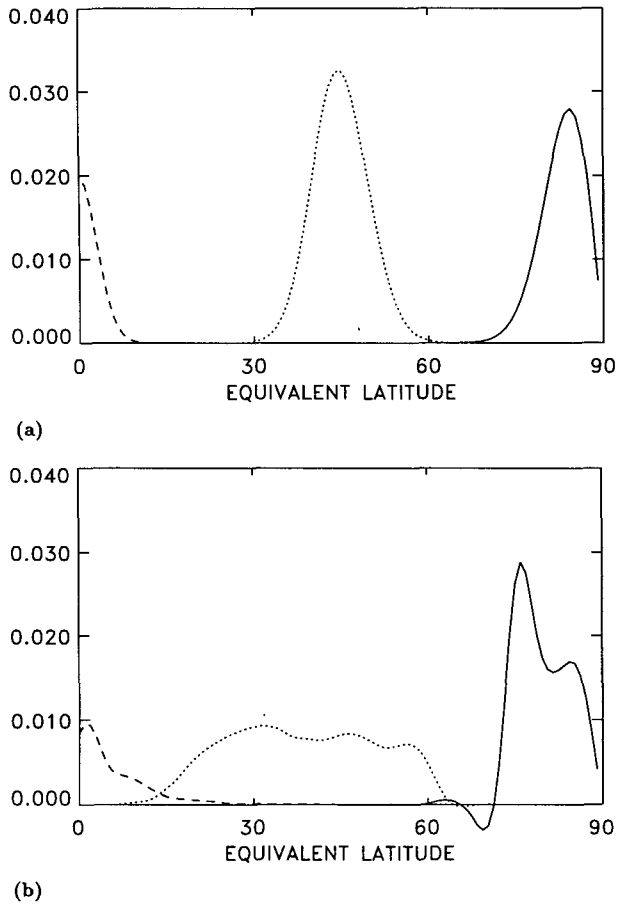

FIG. 11. Amount of tracer (mass-weighted mean tracer times cosine of equivalent latitude) in vortex-following coordinate system as a function of equivalent latitude at (a) day 0; (b) day 80. Tracer A: solid curve, tracer B: dotted curve, and tracer C: dashed curve.

gives us another view of the tendency of tracer B, seen in Fig. 10b, to fill the surf zone. At day 80 we see what appears to be some overlap between tracers A and B. But note also the neighboring negative amount of tracer A. This comes from the numerical tracer-advection inaccuracy associated with the Gibbs fringes noted earlier. Hence the overlap between tracer A and B is largely a numerical artifact, and the result is not meaningful. We also see overlap between tracers B and C. This is more meaningful and reflects the irreversible, quasi-permanent changes brought about by the slow stirring in the tropics seen in Figs. 1, 2. That stirring irreversibly rearranges PV and tracer substances across the nearly zonal coordinate contours in the tropics, giving rise, also, to the slow, deep tropical easterly acceleration seen at bottom right of Figs. 8a,b.

Figure 10b can be compared with Figs. 12 and 13, which are conventional Eulerian zonal, and PV mass-weighted averages of tracer B as a function of time. The area enclosed by PV contours has been converted

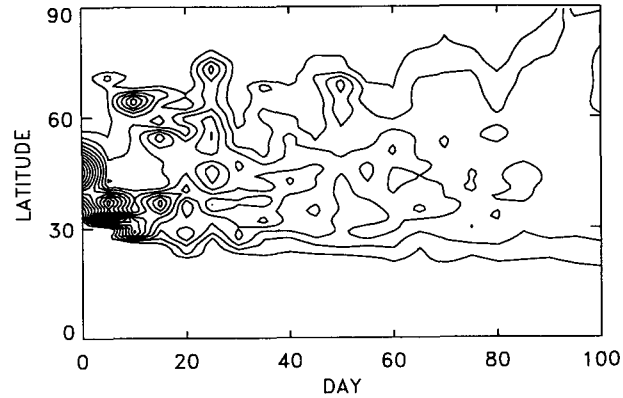

FIG. 12. Eulerian zonal mean of tracer B as function of latitude and time. Contour interval is 0.004.

to an equivalent latitude. The Eulerian zonal average in Fig. 12 shows a spread of tracer B into the subtropics similar to that given by the vortex-following coordinate shown in Fig. 10b, as expected from the near zonality of the vortex-following coordinates there. However, Fig. 12 shows an apparent spread of tracer B right to the pole. This completely obscures the isolation of the vortical air mass.

The PV coordinate average in Fig. 13 does, by contrast, show an isolated vortical air mass, with an area corresponding to the polar cap northward of approximately 60°N. This, as expected, is similar to the result obtained with the vortex-following coordinate in Fig. 10b. However, the PV coordinate average in Fig. 13 shows what looks, misleadingly, like a slower spread of tracer B into the subtropics than in Figs. 10b and 12. This is because tracer B is strongly correlated, up to around day 20, with the PV values corresponding to the initial tracer distribution. The tracer then, very gradually, moves across PV contours and becomes decorrelated with the PV, as a result of diabatic relaxation

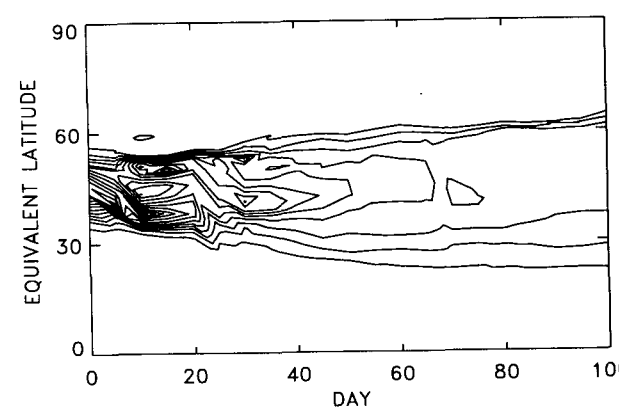

FIG. 13. Mean of tracer B in PV coordinates as function of equivalent latitude and time. Contour interval is 0.004.

acting on the PV, and numerical hyperdiffusion acting both on the PV and on the tracer [cf. the arguments in Hess (1991)].

5. Contour advection applied to the model's velocity field

The Gibbs fringe or hyperdiffusive spreading effects seen in Figs. 3–5 are reminders of well-known difficulties with Eulerian schemes for numerical tracer advection. An alternative approach is to compute the advection of material contours (e.g., Hsu 1980; Lyjak and Smith 1987; JM87). A material contour can be defined by a series of particles that are advected by the velocity field. But, in a velocity field like that produced by the present model integration, there are regions of strong stirring in which adjacent particles on a contour very quickly become separated, and the material contour becomes ill defined.

Here the problem is overcome by introducing the contour advection algorithm. This is part of a sophisticated algorithm, "contour dynamics with surgery," developed by Dritschel (1989) as a means of solving idealized problems in nondivergent barotropic vortex dynamics. It can, however, be applied to any velocity field. From the present viewpoint, its main virtue is an ability to maintain uniform accuracy along the entire length of each material contour, under the control of a single, preassigned error parameter μ. Particles are automatically redistributed along the contour, and new particles added in regions of high curvature, well before the material contour becomes ill defined. Also, special "corner particles" are added when the curvature becomes extreme, as at the end of a thin filament. There is a "surgery" option whereby thin filaments and other features finer than a preassigned scale ϵ can be systematically discarded. The two parameters μ and ϵ together give the user precise control of the tradeoff between accuracy and computational cost; for further details see Dritschel.

Figure 14 shows the first 30-days' evolution of ten initially circular material contours, when advected by the velocity field from the model integration using the contour advection algorithm. The areas between contours have been shaded to make it easy to distinguish different air masses. Here ϵ is taken to be zero (no surgery), and μ to be 0.01, which means that a circular contour around the equator will be described by $2\pi/\mu = 628$ particles. This is much more accurate than most contour dynamics calculations, which are typically performed with $\mu = 0.1$. The particles are redistributed, and added to, twice a day.

The early evolution of the contours looks similar to that of the PV contours in Fig. 1, reflecting the approximate material conservation of PV. At day 10 there is the initial sideways overturning, or folding, of PV contours and material contours in the surf zone. From day 20 to day 30 we see the development of ultrafinescale structure in the surf zone. This does not appear in the model's PV, on which numerical hyperdiffusion acts to damp small scales. The total number of particles defining the ten contours at day 30 has grown to 270 248; cf. 5709 at day 0. The maximum number of particles defining a single contour at day 30 (the one initialized near 37°N) is 68 018; cf. 591 at day 0. This contour has lengthened by nearly a factor of 60 by day 30 and is nearly two million kilometers long.

The accuracy of creating very small scale tracer features from a relatively coarse velocity field could be questioned. However, the key point is that it is the large-scale deformation field that produces the so-called cascade of enstrophy to small scales. Only rarely do coherent structures form at small scales that have a significant effect on the local velocity field for this purpose. The importance of the larger scales is consistent with the fact that a pure deformation field, or pure strain field, has *infinite* spatial scale, yet can shrink advected scales exponentially fast. This is the basis for the "random-straining" models long used in theoretical studies of two-dimensional turbulence (e.g., Batchelor 1952; Kraichnan 1974); it receives further theoretical underpinning from the more recent literature of "chaotic advection" (e.g., Ottino 1989). Examples of the accuracy of contour advection with differently resolved velocity fields are given in the independent work of Waugh and Plumb (1994), strikingly verifying this point.

Figure 15a zooms in on a point in the surf zone, 45°N, 115°W, near the cutoff vortex that is visible also as a high-PV region in Fig. 1, day 30. The diameter of Fig. 15a is 30° latitude, representing a magnification of 6. Figure 15b zooms in further, by another factor 6, on the same point, the diameter of the figure being 5° latitude. The finest structures are of kilometer scale or less. What this might mean in the real stratosphere is discussed below. What is also striking from Fig. 15 is that the fine structure does not occur homogeneously throughout the surf zone. Rather, it occurs in localized regions, in the form of filaments or streaks where contours have been folded back on themselves many times. Conversely, there are places within the surf zone where there has been much less folding, such as the interior of the cutoff vortex.

This could have significant consequences for the modeling of stratospheric chemistry. The high numerical diffusion present in low-resolution chemical models rapidly "mixes" any model filaments. The "mixdown time" of a filament in the real stratosphere could be several days longer. This could be part of what is important in problems like quantifying the amount of ozone destruction that takes place in a filament of chlorine-activated air eroded from the vortex; see, for example, Prather and Jaffe (1990).

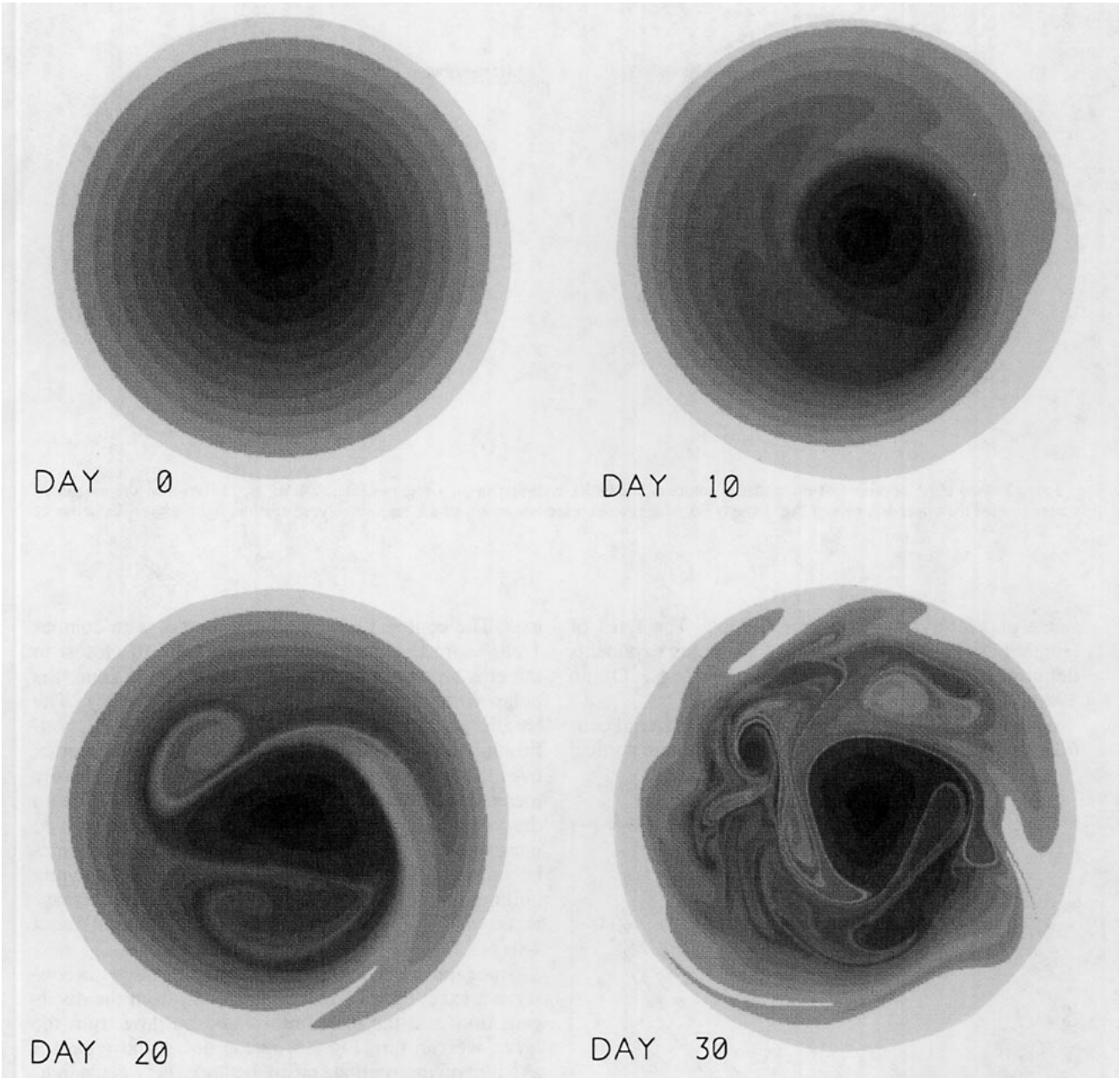

FIG. 14. Contour advection results for ten material contours in integration of Fig. 1 showing days 0 to 30. The areas between contours have been shaded. The initial distribution of contours is equally spaced in sine latitude for the outer nine contours [starting at sin(lat) = 0.1] and the innermost contour is at a latitude of 75°. The outer extremities of the figures represent the equator, and the orientation of the figure is the same as in Fig. 1.

The evolution of the material contours in the surf zone is to be contrasted with the evolution in other regions. For instance, the contour located deepest in the tropics is only slightly folded, indicating relatively weak wave breaking and stirring there. The two contours inside the polar vortex remain almost entirely undular, indicating a remarkable lack of stirring inside the vortex, over the first 30 days at least. We return to this latter question in section 6.

6. Length and distance between the material contours

A quantitative measure of these relative strengths of stirring is the rate of lengthening of each material contour. This is a fundamental measure of "how turbulent" the flow is (e.g., Batchelor 1952; Kraichnan 1974), as opposed to undular, with bounded contour length, corresponding to nonbreaking waves in the

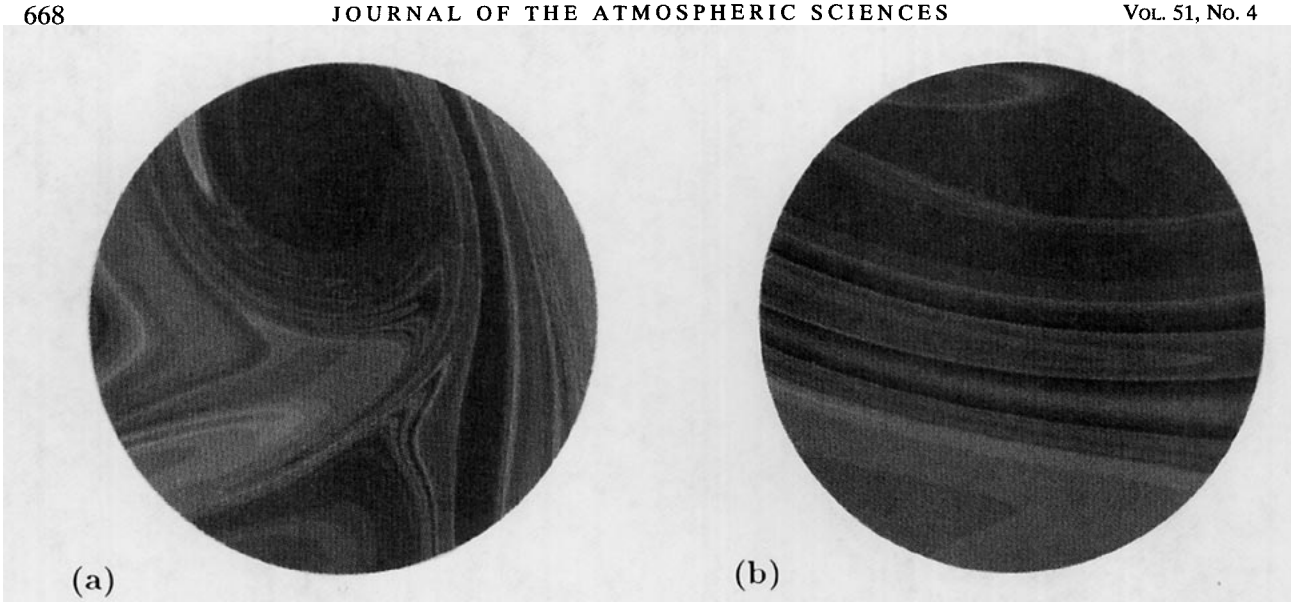

FIG. 15. Two close-up views of the material contours at day 30, zooming in on a region centered at 45°N, 115°W, near the secondary vortex toward the upper left part of Fig. 14, day 30. Magnification factors are 6 and 36, respectively, so that the figures have diameters of 30° and 5°.

sense of McIntyre and Palmer (1985). The rates of lengthening are also related to the Liapunov exponents defined in dynamical-systems theory (e.g., Ottino 1989).

Figure 16 shows the lengths of the ten material contours as functions of time; note the logarithmic vertical axis. The contours have been numbered, with contour 1 closest to the North Pole and contour 10 closest to the equator. The contrasts between the surf zone, the polar vortex, and the tropics show up clearly. The lengths of contours 1 and 2 do not increase at all, confirming the undular behavior inside the polar vortex over the first 30 days. The length of contour 3 hardly increases until day 20, when part of it is eroded from the vortex. The lengths of contours 4 to 8 begin to increase earlier, as soon as Rossby wave amplitudes become large, around day 6. The rates of lengthening build up until, from about day 20 onward, the increase is roughly exponential with an e-folding time of about 4 days.

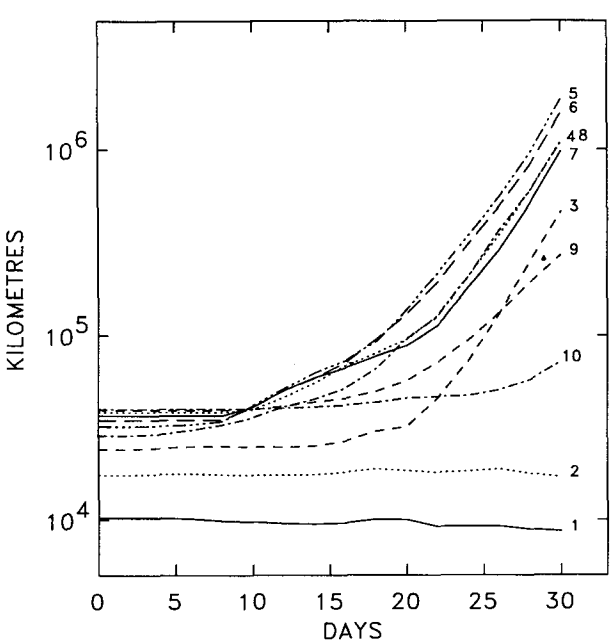

FIG. 16. Length of material contours as a function of time. Curve labeled 1 is contour nearest the north pole, curve labeled 10 is contour nearest the equator. The same plot upside down can be regarded as a plot of mean distance between material contours (see text).

Since the area between neighboring contours is conserved, except for a small contribution from the divergent flow and the mass inflow and outflow from the layer, we can turn Fig. 16 upside down and regard it as a plot of approximate mean distances between neighboring contours or contour separations. We can also look at *minimum* contour separations. In Fig. 17, the curve labeled 1 shows the minimum separation between contours 1 and 2, and so on. Curves 1, 2, and 9 show little decrease over the 22 days plotted, consistent with undular behavior, or wave breaking that is weak. The other curves all show the clear and persistent decrease that can be expected in the surf zone. From about day 16 onward the rates of decrease become very rapid, with a shortest e-folding time just under one day. Minimum contour separations are down to a few kilometers or less by day 22. Even the contour advection algorithm, at practically attainable accuracies, cannot locate contours much more accurately than this. We recall 1) that the implied scales are already small enough for the

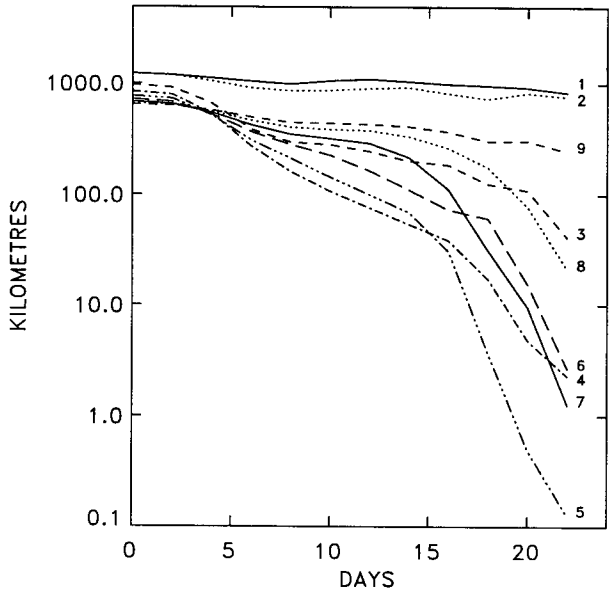

FIG. 17. Minimum distance between material contours as a function of time up to day 22. Curve labeled 1 is minimum distance between contours 1 and 2, curve labeled 2 is minimum distance between contours 2 and 3, etc.

corresponding vertical scales in the real stratosphere (compressed by Prandtl's ratio $f/N \sim 10^{-2}$, where f is the Coriolis parameter and N the buoyancy frequency) to begin to feel molecular diffusion (JM87), and 2) that small-scale, three-dimensional turbulence will probably have intervened earlier (Dewan 1981; Woodman and Rastogi 1984; McIntyre 1990).

Figure 18 shows contours 1 and 2 at 80 and 100 days, highlighting the very different situation within the model vortex. It is remarkable that contour 2 has remained almost perfectly undular up to day 80, showing that the vortex interior, at least the part of it within contour 2, has remained not approximately, but perfectly, isolated, according to this model, up to day 80. This is even after the long sequence of highly aperiodic, large amplitude disturbances to which the vortex was subjected to by then. Similarly remarkable vortex-core isolation effects have been seen in the idealized two-dimensional vortex studies of Dritschel and Legras (1993).

Figure 18, day 100, on careful inspection, shows that, despite the very violent disturbance to the vortex on day 100, with which the polar easterlies in Fig. 8b are associated, part of contour 2 still encloses an isolated core with only a single, very thin filament now being eroded outward.

Contour 1, on the other hand, has by day 80 ceased to behave undularly; there is very slow mixing within the isolated core of the vortex. It is far too slow to be regarded as Rossby wave breaking, as defined by McIntyre and Palmer (1984, 1985); the irreversible contour deformation is not rapid, in the sense of taking place on the time scale ω^{-1} associated with intrinsic Rossby wave frequencies ω (meaning that $2\pi/\omega$ is a typical time for a material particle to travel through one wavelength, of order a few days in this experiment).

7. Discussion

The vortex-following coordinate averages and the contour advection results have between them given us

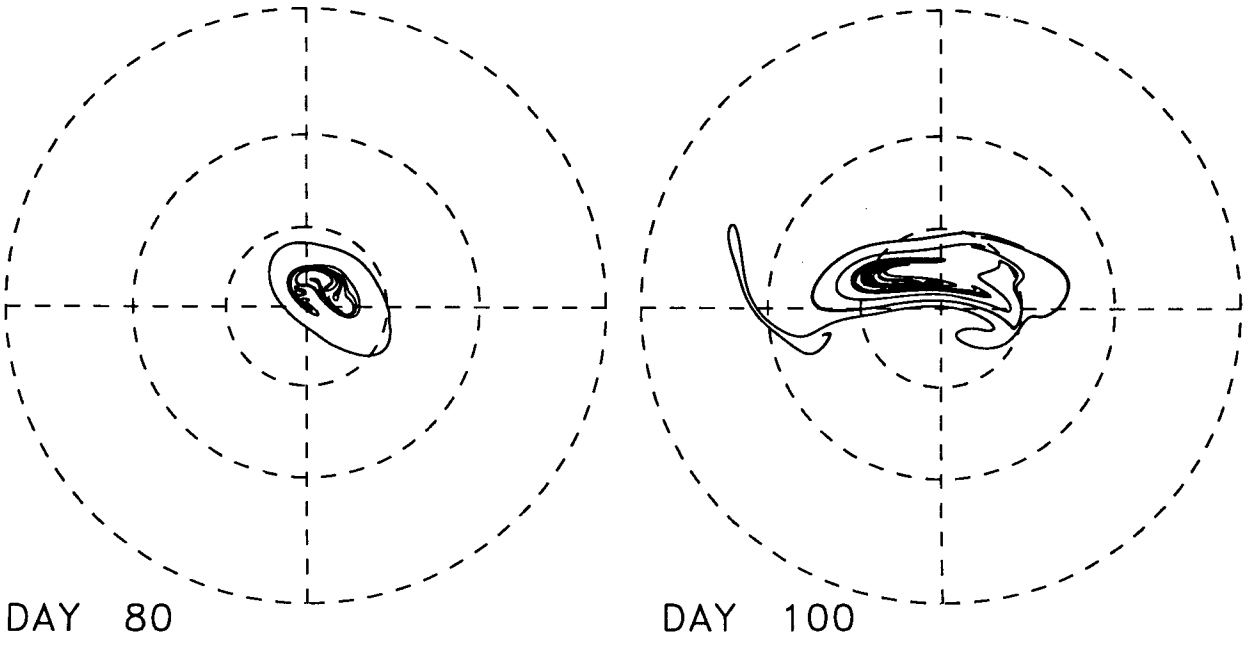

FIG. 18. Contour advection results for two innermost contours of Fig. 14, contours 1 and 2, at days 80 and 100.

a clearer view of the airmass transport, or lack of it, between different regions in the model. One example is the complete isolation of the vortex core just noted. Another is the transport of subtropical or tropical air into the surf zone, discussed near the end of section 3.

Figure 14 shows another example of this very clearly. On day 20, a mass of low-PV tropical air has been advected round the polar vortex and has accumulated near 45°N, 135°W, where it has formed a quasi-Aleutian anticyclone. By day 30 (again see Fig. 14), this air mass has been stirred down to small scales. On day 30, however, another tropical air mass, which originated equatorward of 12°N, can be seen near 30°N, 160°E. On day 20 this same air can be seen being drawn in round the polar vortex near 40°N, 120°E.

These events in which tropical or subtropical air is drawn in round the vortex are robust enough to be seen, also, by close examination of the Eulerian tracer diagnostics in section 3. They occur repeatedly over the 100-day integration. They happen whenever the vortex moves off the pole. Similar pulsed transport events have been reported in other model and observational studies, for example, in the barotropic model study of J89, in the GCM study of Mahlman and Umscheid (1987), and in the observational study of Leovy et al. (1985) in which such transport events were first seen in LIMS ozone data. They appear to be a robust feature of the real stratosphere and of many stratospheric models. Such events, describable as subtropical erosion by the action of the polar vortex rather than by smaller-scale surf-zone eddies, are probably the main mechanism by which tropical air is transported into middle latitudes.

The converse phenomenon, airmass transport by erosion of material from the polar vortex into the surf zone, is a relatively weak effect. There is no action of the tropics upon the polar vortex that seems comparable to the action of the polar vortex upon the tropics. Also, the PV gradients in the edge of the vortex are much stronger than those in the subtropics, hence PV contours are more "elastic" and less likely to deform irreversibly. Typical vortex erosion events can be seen taking place on day 30, for instance, in Fig. 1 and, with special clarity, in Fig. 14, near 40°N, 100°E and 50°N, 10°E. It is obvious that these events involve relatively small amounts of air. By comparing Fig. 14 and 18, by noting the smallness of the area of the eroded part of contour 2 in Fig. 18, day 100, and by noting also the relatively modest diabatic mass flow rates implied by Fig. 9, we see that the total amount of air eroded from the vortex between days 30 and 100 cannot be much greater, in order of magnitude, than the amount corresponding to the lightest-shaded part of the vortex as it appears on day 30 in Fig. 14.

We can get a sufficient idea of orders of magnitude by comparing areas, since the relevant fractional layer depth changes are of order 25%. The area δA of the lightest-shaded part of the vortex on day 30 is the area contained between contour 2 and the noneroded part of contour 3. This area δA is 40% of the area of the vortex at day 30, counting the latter as the total area enclosed by the noneroded part of contour 3. The area δA is only 16% of the area of the surf zone, taken from Fig. 7 as corresponding roughly to the area between 30°N and 60°N.

These orders of magnitude are of interest in connection with the "flowing processor hypothesis" already referred to in section 1. Tuck (1989) suggests that the air fed through the vortex can explain the observed dryness of the Southern Hemispheric lower stratosphere; see also the recent discussion by Randel (1993). Tuck et al. (1992) suggest that the rate of erosion of chlorine-activated air from the real lower-stratospheric vortex, as suggested by small-scale features seen on isentropic maps of PV obtained from ECMWF analyses, may be enough to be significant for midlatitude ozone destruction. Now we must be extremely cautious about extrapolating the present single-layer model results to the real lower stratosphere, if only because of the incomplete modeling of diabatic, radiative heating and cooling near the vortex edge (e.g., Haynes and Ward 1993), and the incomplete modeling of the stirring from the tops of tropospheric synoptic-scale eddies. These factors might change the picture somewhat. However, two points about the present results seem robust, and probably do apply to the real lower stratosphere.

The first is the *relative* order of magnitude of the erosion rates: that erosion from the tropics into the surf zone is relatively strong compared with erosion from the vortex into the surf zone. The fluid dynamical reasons for this asymmetry, the action of the displaced polar vortex on the subtropics, have already been indicated. From LIMS (e.g., see WMO 1985, chapter 9) a large tropical reservoir of dry air was observed in the lower stratosphere. So the possibility that the drying of the Southern Hemisphere midlatitudes might be coming mostly from the tropics should not be ruled out.

The second point is simply the small order of magnitude of vortex erosion rates. The flowing processor hypothesis, or at least the version of it that relies on erosion to bring vortex air out to middle latitudes (Tuck et al. 1992), would require erosion rates in the order of six times higher than indicated by the integration here. It can be added that the small-scale features seen on the aforementioned isentropic maps of PV bear no resemblance to the flow features in any high-resolution fluid dynamical model, for example, as seen in Figs. 1, 2, and 14. Work is presently in hand to apply the contour advection algorithm to the velocity fields of some relatively realistic high-resolution, three-dimensional model simulations; it is hoped that these might provide the first credible quantitative estimates of subpolar and subtropical erosion rates in the real lower stratosphere.

The present work has also demonstrated a new approach to quantifying the properties of quasi-horizon-

tal, isentropic stirring, and to refining our estimates of "mixdown times," or time delays to chemical contact between previously separated constituents. See the remarks toward the end of section 5, and in section 6 in connection with Figs. 16 and 17. Again, it is hoped that corresponding results will soon be obtained from the velocity fields of high-resolution, three-dimensional models, and that they will be able to be combined with models like those of Dewan (1981) and Woodman and Rastogi (1984) of the vertical mixing by intermittent small-scale clear-air turbulence, to refine our ideas about mixing in the lower stratosphere and its chemical consequences. Such estimates could assume added importance, because of newly revived concerns about the effects of aircraft emissions on the lower stratosphere, where chemical concentrations evolve by many orders of magnitude, and mixdown could prove to be a significant aspect.

Acknowledgments. I am grateful to my colleagues who have provided the stimulus for this work carried out in the Atmospheric Dynamics Group, Department of Applied Mathematics and Theoretical Physics. I thank C. J. Cooper, S. P. Cooper, J. C. Farman, P. H. Haynes, M. E. McIntyre, A. O'Neill, R. Saravanan, and R. Sutton for many discussions of the scientific background and for help in various ways. I thank also M. R. Schoeberl and two anonymous reviewers for their comments on the paper, which have led to significant strengthening of the results and discussion. Most especially I would like to thank D. G. Dritschel for generously making available his contour dynamics code at an early stage of this research, and M. N. Juckes for generous initial help with the Reading shallow-water equation model. The work was supported in part by the U.K. Natural Environment Research Council through the U.K. Universities' Global Atmospheric Modelling Programme, through a British Antarctic Survey Special Topic grant and through a Capital Equipment grant, and by the Innovative Science and Technology Program through grants administered by the U.S. Navy, all of whom, together with the National Computer Centres at the Rutherford Appleton Laboratory and at the University of London Computing Centre, have provided generous contributions toward computing resources. The Special Topic grant funded my position as a British Antarctic Survey Research Fellow held between 1 July 1989 and 30 November 1992.

APPENDIX

Definition of the Vortex-Following Coordinate System

Choose a PV contour embedded in the edge of the vortex, as characterized by steep PV gradients and reversible, undular contour deformations. Call this PV contour the "key contour." Let the longitude and latitude of the centroid of the key contour be (λ_0, ϕ_0). Let the area enclosed by the key contour be A, so that its equivalent latitude ϕ_k, defined to correspond to the area it encloses, is

$$\phi_k = \sin^{-1}\left(1 - \frac{A}{2\pi a^2}\right), \tag{A1}$$

where a is the earth's radius. Introduce rotated spherical coordinates (λ_r, ϕ_r), whose "north pole"—let us call it the "rotated north pole"—is placed at the centroid of the key contour, and whose zero of rotated longitude, $\lambda_r = 0$, is in the meridional plane corresponding to true longitude $\lambda = \lambda_0$.

In the rotated coordinate system, let the shape of the key contour be described by the function $\phi_r = \Phi(\lambda_r)$, say, specifying the rotated latitude ϕ_r of a point on the key contour whose rotated longitude is λ_r. It is important that the key contour should not be too close to the outer edge of the vortex, because if the contour is being eroded, and hence folded sideways, then $\Phi(\lambda_r)$ might not be a single-valued function. We can rescale the function $\Phi(\lambda_r)$, and shift its origin, to give another function

$$F(\lambda_r) = \frac{\Phi(\lambda_r) - \phi_k}{\pi/2 - \phi_k} \tag{A2}$$

also describing the shape of the key contour, in a way that will prove convenient.

It will also prove convenient to let each coordinate contour be labeled by a parameter ψ, which we call the pseudolatitude and will take values 0, ϕ_κ, and $\pi/2$ for the coordinate contours coinciding respectively with the equator, the key contour, and the centroid of the key contour. Define the function

$$\alpha(\psi) = \min(1, \psi/\phi_k); \tag{A3}$$

this will be used to specify the amount of distortion of the coordinate contours from circular shapes.

As ψ and $\alpha(\psi)$ approach zero, the coordinate contour labeled by ψ becomes more nearly circular; and we want the center of the coordinate contour to approach the true north pole so that the contour itself can approach the equator, as illustrated in Fig. 6. To this end, somewhat arbitrarily, we take a new set of rotated spherical coordinates $(\hat{\lambda}_r, \hat{\phi}_r)$ that coincides with the original rotated coordinates whenever $\alpha = 1$, that is, whenever $\psi \geq \phi_\kappa$, but otherwise has its rotated north pole not at true longitude and latitude (λ_0, ϕ_0) but rather at, say, (λ_0, ϕ_α), where

$$\phi_\alpha = \phi_\alpha(\psi) = \pi/2 - \alpha^{0.7}(\pi/2 - \phi_0). \tag{A4}$$

As before, the zero of the new rotated longitude, $\hat{\lambda}_r = 0$, is chosen to be in the meridional plane corresponding to true longitude $\lambda = \lambda_0$. The shape of the coordinate contour labeled by ψ is now defined by specifying its new rotated latitude $\hat{\phi}_r$, relative to the new rotated north pole, to be, again somewhat arbitrarily, the following function of the new rotated longitude $\hat{\lambda}_r$:

$$\hat{\phi}_r(\hat{\lambda}_r; \psi) = \psi + \alpha^{1.5} F(\hat{\lambda}_r)(\pi/2 - \psi). \quad \text{(A5)}$$

These definitions (A4) and (A5) have an ad hoc character, but tests have shown that the resulting coordinate averages, such as the average defined by (4), are not sensitive to the particular function of α chosen in (A4) and (A5).

We can label each coordinate contour, alternatively, by an equivalent latitude ϕ_e, defined from the enclosed area in the same way as in (A1). Computations show that, for each coordinate contour, the equivalent latitude, ϕ_e, is close in numerical value to the pseudolatitude, ψ. Although it is ψ that is used in the computations, in the manner just implied, the results of those computations are plotted against ϕ_e in Figs. 7–11.

The foregoing is enough to define the vortex-following coordinate system, and the results plotted in Figs. 7–11. However, for completeness, we note the explicit transformations that express the coordinate contour shapes in terms of true longitude and latitude.

For the coordinate contour labeled by ψ, first introduce a special set of Cartesian coordinates $(\hat{x}, \hat{y}, \hat{z})$ whose origin is at the earth's center, whose unit of length is the earth's radius, and whose $\hat{z}$ axis goes through the rotated north pole of the contour, that is, through the point whose true longitude and latitude are $\{\lambda_0, \phi_\alpha(\psi)\}$. The $\hat{x}$ axis is chosen to coincide with $\hat{\lambda}_r = 0$. In these coordinates, the shape of the coordinate contour labeled by pseudolatitude ψ is given by the locus, as $\hat{\lambda}_r$ runs from 0 to 2π, of

$$\hat{x} = \cos\{\hat{\phi}_r(\hat{\lambda}_r; \psi)\} \cos(\hat{\lambda}_r), \quad \text{(A6a)}$$

$$\hat{y} = \cos\{\hat{\phi}_r(\hat{\lambda}_r; \psi)\} \sin(\hat{\lambda}_r), \quad \text{(A6b)}$$

$$\hat{z} = \sin\{\hat{\phi}_r(\hat{\lambda}_r; \psi)\}. \quad \text{(A6c)}$$

Now transform this to a similar Cartesian coordinate system (x, y, z) whose z axis goes through the true north pole and whose x axis coincides with zero true longitude, $\lambda = 0$. Suppressing the functional dependence on $(\hat{\lambda}_r; \psi)$, we get

$$x = \cos(\lambda_0)(\hat{x} \sin(\phi_\alpha) + \hat{z} \cos(\phi_\alpha)) + \hat{y} \sin(\lambda_0), \quad \text{(A7a)}$$

$$y = -\sin(\lambda_0)(\hat{x} \sin(\phi_\alpha) + \hat{z} \cos(\phi_\alpha)) + \hat{y} \cos(\lambda_0), \quad \text{(A7b)}$$

$$z = \hat{z} \sin(\phi_\alpha) - \hat{x} \cos(\phi_\alpha). \quad \text{(A7c)}$$

So, finally, the shape of the coordinate contour labeled by ψ is given by the locus, as $\hat{\lambda}_r$ runs from 0 to 2π, of the point whose true longitude and latitude are

$$\lambda = \tan^{-1}(y/x), \quad \text{(A8a)}$$

$$\phi = \sin^{-1}(z), \quad \text{(A8b)}$$

where it is understood that (A7) is used to substitute for x, y, z and then (A6) for $\hat{x}, \hat{y}, \hat{z}$.

REFERENCES

Al-Ajmi, D. N., R. S. Harwood, and T. Miles, 1985: A sudden warming in the middle atmosphere of the Southern Hemisphere. *Quart. J. Roy. Meteor. Soc.*, **111,** 359–389.

Batchelor, G. K., 1952: The effect of homogeneous turbulence on material lines and surfaces. *Proc. Roy. Soc. London,* **A213,** 349–366.

Butchart, N., and E. E. Remsberg, 1986: Area of the stratospheric polar vortex as a diagnostic for tracer transport on an isentropic surface. *J. Atmos. Sci.,* **43,** 1319–1339.

Clough, S. A., N. S. Grahame, and A. O'Neill, 1985: Potential vorticity in the stratosphere derived using data from satellites. *Quart. J. Roy. Meteor. Soc.,* **111,** 335–358.

Dewan, E. M., 1981: Turbulent vertical transport due to thin intermittent mixing layers in the stratosphere and other stable fluids. *Science,* **211,** 1041–1042.

Dritschel, D. G., 1989: Contour dynamics and contour surgery: Numerical algorithms for extended, high-resolution modelling of vortex dynamics in two-dimensional, inviscid, incompressible flows. *Computer Phys. Rep.,* **10,** 78–146.

——, and B. Legras, 1993: On the structure of isolated, coherent vortices in a two-dimensional, incompressible fluid at very high Reynolds numbers. *J. Fluid Mech.,* submitted.

Fels, S. B., 1985: Radiative–dynamical interactions in the middle atmosphere. *Advances in Geophysics: Issues in Atmospheric and Oceanic modelling (28A),* S. Manabe, Ed. Academic Press, 277–300.

Haynes, P. H., C. J. Marks, M. E. McIntyre, T. G. Shepherd, and K. P. Shine, 1991: On the "downward control" of extratropical diabatic circulations by eddy-induced mean zonal forces. *J. Atmos. Sci.,* **48,** 651–678.

——, and W. E. Ward, 1993: The effect of realistic radiative transfer on potential vorticity structures, including the influence of background shear and strain. *J. Atmos. Sci.,* **50,** 3431–3453.

Hess, P. G., 1991: Mixing processes following the final stratospheric warming. *J. Atmos. Sci.,* **48,** 1625–1641.

Hsu, C.-P. F., 1980: Air parcel motions during a numerically simulated sudden stratospheric warming. *J. Atmos. Sci.,* **37,** 2768–2792.

Juckes, M. N., 1989: A shallow water model of the winter stratosphere. *J. Atmos. Sci.,* **46,** 2934–2955.

——, and M. E. McIntyre, 1987: A high resolution, one-layer model of breaking planetary waves in the stratosphere. *Nature,* **328,** 590–596.

Kraichnan, R. H., 1974: Convection of a passive scalar by a quasi-uniform random straining field. *J. Fluid Mech.,* **64,** 737–762.

Legras, B., and D. G. Dritschel, 1993: A comparison of the contour surgery and pseudospectral methods. *J. Comput. Phys.,* **104,** 287–302.

Leovy, C. B., C.-R. Sun, M. H. Hitchman, E. E. Remsberg, J. M. Russell III, L. L. Gordley, J. C. Gille, and L. V. Lyjak, 1985: Transport of ozone in the middle stratosphere: Evidence for planetary wave breaking. *J. Atmos. Sci.,* **42,** 230–244.

Lyjak, L. V., and A. K. Smith, 1987: Lagrangian mean circulations in the stratosphere. *J. Atmos. Sci.,* **44,** 2252–2266.

Mahlman, J. D., and L. J. Umscheid, 1987: Comprehensive modeling of the middle atmosphere: The influence of horizontal resolution. *Transport Processes in the Middle Atmosphere.* (NATO Workshop November 1986 at Erice, Sicily), G. Visconti, R. R. Garcia, Eds. Reidel, 251–266.

McCormick, M. P., and R. E. Veiga, 1992: SAGE II measurements of early Pinatubo aerosols. *Geophys. Res. Lett.,* **19,** 155–158.

McIntyre, M. E., 1980: Towards a Lagrangian-mean description of stratospheric circulations and chemical transports. *Philos. Trans. Roy. Soc. London,* **A296,** 129–148.

——, 1982: How well do we understand the dynamics of stratospheric warmings? *J. Meteor. Soc. Japan,* **60,** 37–65.

——, 1990: Middle atmospheric dynamics and transport: Some current challenges to our understanding. *Dynamics, Transport and*

Photochemistry in the Middle Atmosphere of the Southern Hemisphere: San Francisco NATO Workshop, A. O'Neill, Ed., Kluwer Academic Publishers, 1–18.

——, and T. N. Palmer, 1983: Breaking planetary waves in the stratosphere. *Nature,* **305,** 593–600.

——, and ——, 1984: The "surf zone" in the stratosphere. *J. Atmos. Terr. Phys.,* **46,** 825–849.

——, and ——, 1985: A note on the general concept of wave breaking for Rossby and gravity waves. *Pure Appl. Geophys.,* **123,** 964–975.

Ottino, J. M., 1989: *The Kinematics of Mixing: Stretching, Chaos and Transport.* Cambridge University Press, 378 pp.

Palmer, T. N., and C.-P. F. Hsu, 1983: Stratospheric sudden coolings and the role of nonlinear wave interactions in preconditioning the circumpolar flow. *J. Atmos. Sci.,* **40,** 909–928.

Prather, M. J., and A. H. Jaffe, 1990: Global impact of the Antarctic ozone hole: Chemical propagation. *J. Geophys. Res.,* **95,** 3473–3492.

Polvani, L. M., and R. A. Plumb, 1992: Rossby wave breaking, microbreaking, filamentation and secondary vortex formation: The dynamics of a perturbed vortex. *J. Atmos. Sci.,* **49,** 462–476.

Proffitt, M. H., K. K. Margitan, K. K. Kelly, M. Loewenstein, J. R. Podolske, and K. R. Chan, 1990: Ozone loss in the Arctic polar vortex inferred from high-altitude aircraft measurements. *Nature,* **347,** 31–36.

Randel, W., 1993: Ideas flow on Antarctic vortex. *Nature,* **364,** 105–106.

Salby, M. L., D. O'Sullivan, R. R. Garcia, and P. Callaghan, 1990: Air motions accompanying the development of a planetary wave critical layer. *J. Atmos. Sci.,* **47,** 1179–1204.

Schoeberl, M. R., L. R. Lait, P. A. Newman, R. L. Martin, M. H. Proffitt, D. L. Hartmann, M. Loewenstein, J. Podolske, S. E. Strahan, J. Anderson, K. R. Chan, and B. Gary, 1989: Reconstruction of the constituent distribution and trends in the Antarctic polar vortex from ER-2 flight observations. *J. Geophys. Res.,* **94,** 16 815–16 846.

——, ——, ——, and J. E. Rosenfield, 1992: The structure of the polar vortex. *J. Geophys. Res.,* **97**(D8), 7859–7882.

Solomon, S., 1990: Progress towards a quantitative understanding of Antarctic ozone depletion. *Nature,* **347,** 347–353.

Stolarski, R. S., P. Bloomfield, R. D. McPeters, and J. R. Herman, 1991: Total ozone trends deduced from Nimbus 7 TOMS data. *Geophys. Res. Lett.,* **18,** 1015–1018.

——, R. Bojkov, L. Bishop, C. Zerefos, J. Staehlin, and J. Zawodny, 1992: Measured trends in stratospheric ozone. *Science,* **256,** 342–349.

Stowe, L. L., P. P. Pellegrino, and R. M. Carey, 1992: Monitoring the Mt. Pinatubo aerosol layer with NOAA/11 AVHRR data. *Geophys. Res. Let.,* **19,** 159–162.

Tuck, A. F., 1989: Synoptic and chemical evolution of the Antarctic vortex in late winter and early spring, 1987. *J. Geophys. Res.,* **94,** 11 687–11 737.

——, T. Davies, S. J. Hovde, M. Noguer-Alba, D. W. Fahey, S. R. Kawa, K. K. Kelly, D. M. Murphy, M. R. Proffitt, J. J. Margitan, M. Loewenstein, J. R. Podolske, S. E. Strahan, and K. R. Chan, 1992: Polar stratospheric cloud processed air and potential vorticity in the Northern Hemisphere lower stratosphere at mid-latitudes during winter. *J. Geophys. Res.,* **97**(D8), 7883–7904.

Waugh, D. W., and R. A. Plumb, 1994: Contour advection with surgery: A technique for investigating finescale structure in tracer transport. *J. Atmos. Sci.,* **51,** 530–540.

WMO, 1985: *Atmospheric Ozone 1985: Assessment of Our Understanding of the Processes Controlling Its Present Distribution and Change.* World Meteorological Organization Global Ozone Research and Monitoring Project Report No. 16, 3 volumes. World Meteorological Organization, 1095 + 86 pp.

Woodman, R. F., and P. K. Rastogi, 1984: Evaluation of effective eddy diffusive coefficients using radar observations of turbulence in the stratosphere. *Geophys. Res. Lett.,* **11,** 243–246.